

Supporting Material: Low temperature multimode atomic force microscopy using an active MEMS cantilever

Michael G. Ruppert,^{*,†} Miguel Wiche,[‡] André Schirmeisen,[‡] and Daniel
Ebeling^{*,‡}

[†]*University of Technology Sydney, Centre for Audio, Acoustics and Vibration, Ultimo,
NSW 2007, Australia*

[‡]*Justus Liebig University Giessen, Institute of Applied Physics, Giessen, 35392, Germany*

E-mail: michael.ruppert@uts.edu.au; daniel.ebeling@ap.physik.uni-giessen.de

Piezoelectric MEMS Cantilever Amplitude Calibration

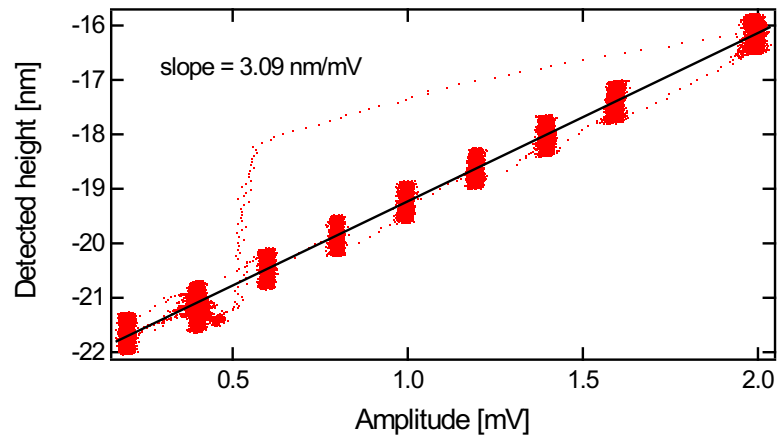


Figure S1: Amplitude calibration of the first mode of the piezoelectric MEMS cantilever. Oscillation amplitude was stepped from 0.2 mV to 2 mV in 0.2 mV steps.

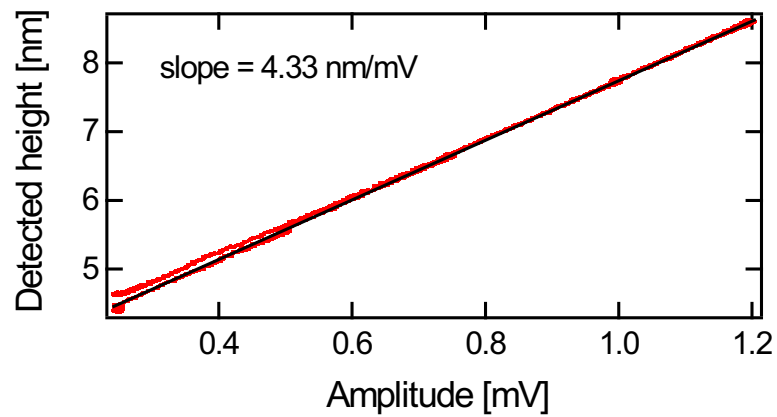


Figure S2: Amplitude calibration of the third mode of the piezoelectric MEMS cantilever. Oscillation amplitude was stepped from 0.25 mV to 1.2 mV in 0.25 mV steps.

LT-AFM/STM Images with Piezoelectric MEMS Cantilever (Mode 3) at Varying Imaging Speeds

Combined STM/AFM imaging results on the third mode of the piezoelectric MEMS cantilever at varying imaging speeds are shown in Figure S3. Single atomic defects in the Au(111) herringbone reconstruction are visible in all STM images, even for high imaging speeds. Frequency shift images clearly identify the Au(111) herringbone reconstruction, even for high imaging speeds (Figure S3(f)). Frequency shift images resolve the atomic defects at an imaging speed of 50 nm/s (Figure S3(g)) and slower.

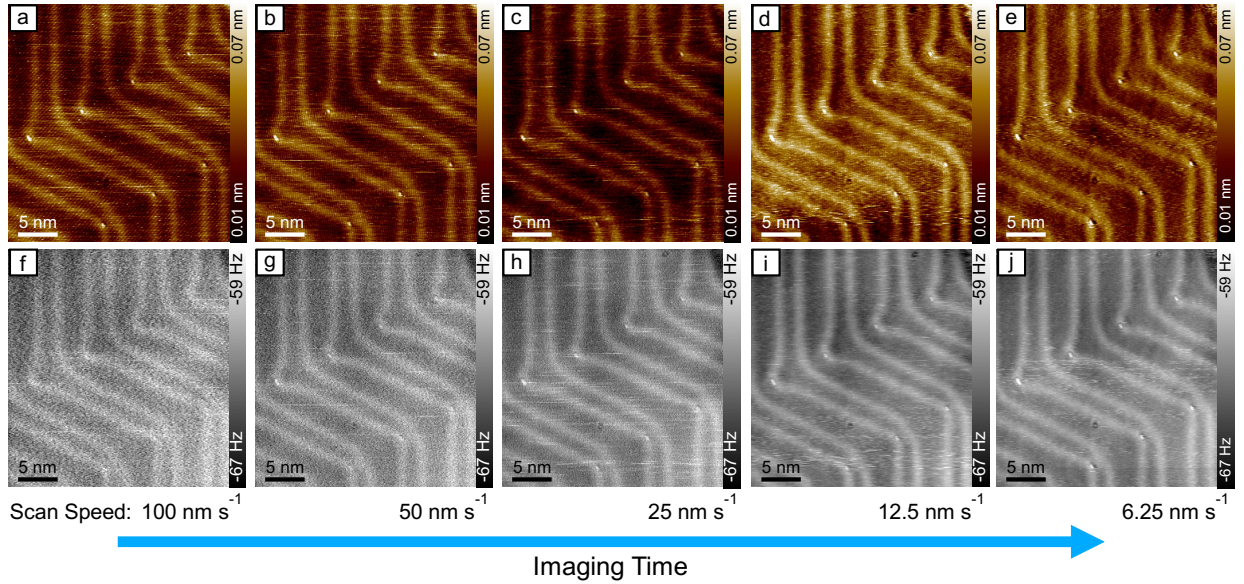


Figure S3: LT-AFM/STM image obtained with the third mode of the piezoelectric MEMS cantilever of the Au(111) herringbone reconstruction. Imaging conditions: $I_t = 30$ pA, $V = 100$ mV, image size = 30×30 nm, 300×300 pixel, $A_0 = 1.08$ nm. The images were recorded at different raster times (RT): (a and f) 1 ms/pixel, (b and g) 2 ms/pixel, (c and h) 4 ms/pixel, (d and i) 8 ms/pixel and (e and j) 16 ms/pixel. Corresponding scan speeds are mentioned in the image. For $RT < 8$ ms/pixel, the PLL bandwidth was set to 50 Hz. For $RT \geq 8$ ms/pixel, the PLL bandwidth was set to 10 Hz.

LT-AFM/STM Images with qPlus Sensor (Mode 1) at Varying Imaging Speeds

A combined STM/AFM image series at varying imaging speeds has been recorded with a conventional qPlus sensor with Tungsten wire tip and is shown in Figure S4. Single atomic defects in the Au(111) herringbone reconstruction are clearly visible in all STM images, however, frequency shift images only resolve the Au(111) herringbone reconstruction in Figure S4(i) and Figure S4(j) (at an imaging speed of 12.5 nm/s and slower).

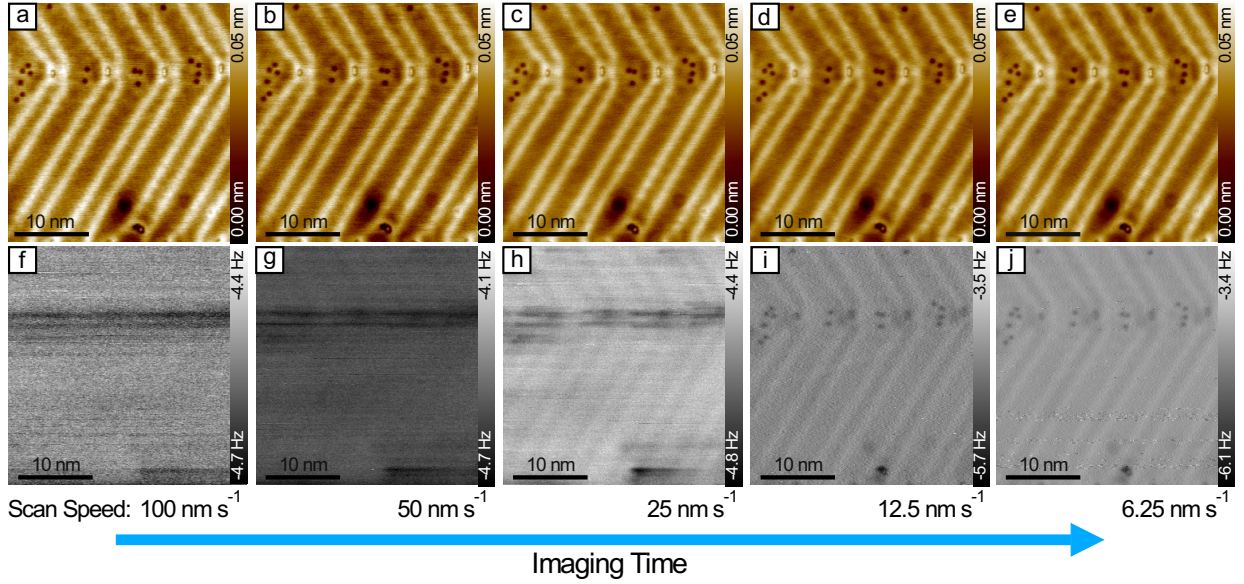


Figure S4: LT-AFM/STM images obtained with a qPlus sensor of the Au(111) herringbone reconstruction. Imaging conditions: $I_t = 30$ pA, $V = 100$ mV, image size = 30×30 nm, 300×300 pixel, $A_0 = 52$ pm ($400 \mu\text{V}$), $f_0 = 26.98$ kHz and $Q \approx 51,000$. The images were recorded at different raster times (RT): (a and f) 1 ms/pixel, (b and g) 2 ms/pixel, (c and h) 4 ms/pixel, (d and i) 8 ms/pixel and (e and j) 16 ms/pixel. Corresponding scan speeds are mentioned in the image. For $RT < 8$ ms/pixel, the PLL bandwidth was set to 50 Hz. For $RT \geq 8$ ms/pixel, the PLL bandwidth was set to 10 Hz.

High Resolution LT-AFM/STM Images with qPlus Sensor (Mode 1) at Low Imaging Speed

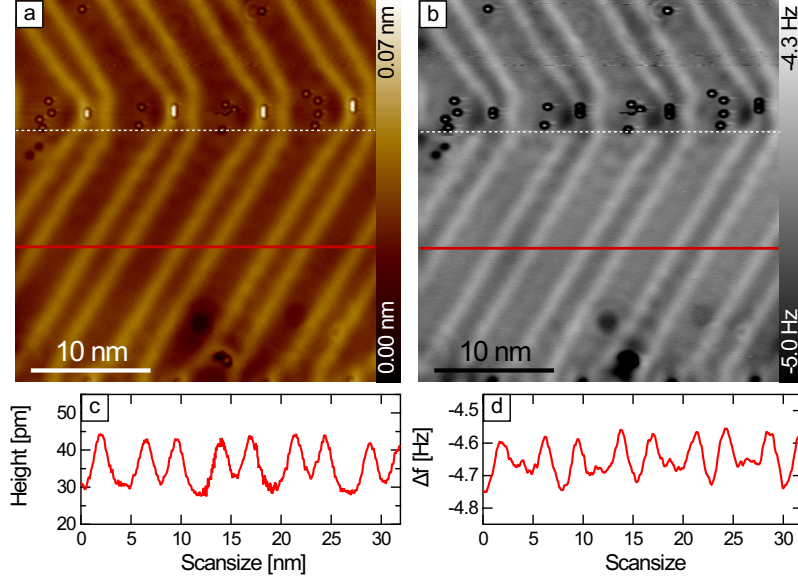


Figure S5: High-resolution LT-AFM/STM image obtained with a qPlus sensor of the Au(111) herringbone reconstruction showing (a) STM image, (b) frequency-shift image, (c) cross-section of (a), and (d) cross-section of (b). Imaging conditions: $I_t = 50$ pA, $V = 100$ mV, image size = 30×30 nm, 600×600 pixel, raster time = 30 ms/pixel, scan speed = 1.67 nm/s, $A_0 = 52$ pm (400 μ V), $f_0 = 26.98$ kHz and $Q \approx 51,000$. The PLL bandwidth was set to 1 Hz. A CO molecule was picked up during scanning. The dashed white line indicates the transition from metal tip to CO tip.

Determining the Effective Signal-to-noise Ratio (SNR) for STM Topography and AFM Frequency Shift Images

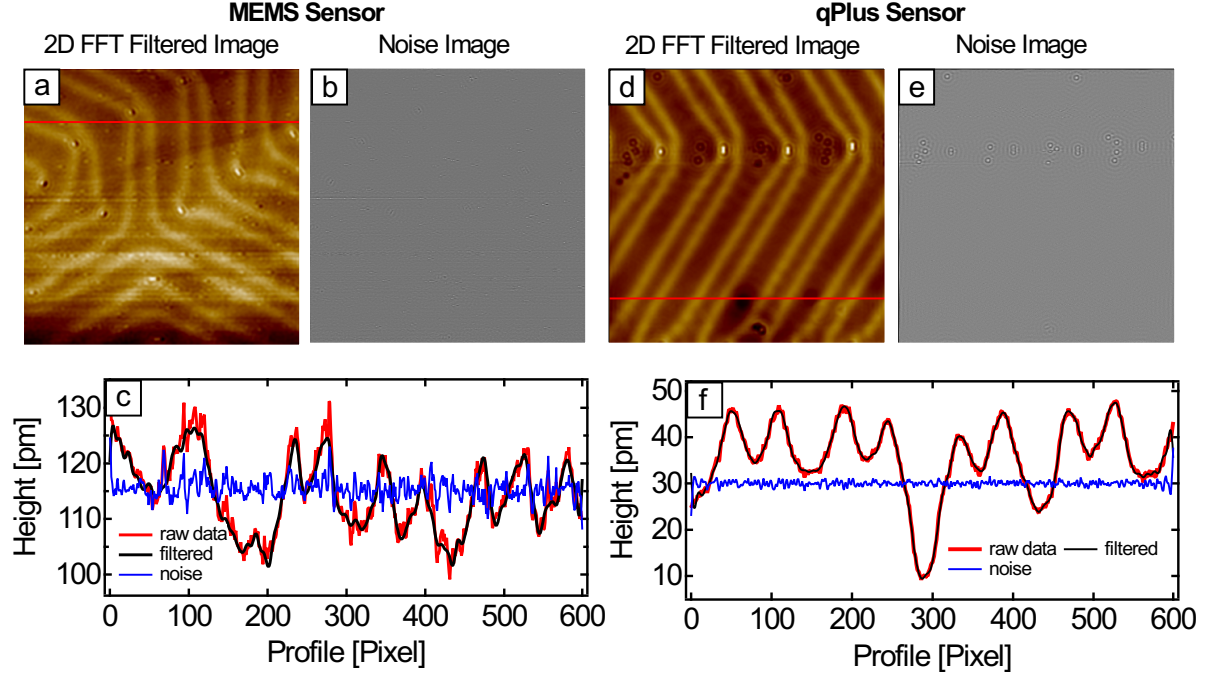


Figure S6: Effective SNR calculation from STM topography images for the MEMS sensor (Mode 3) and a qPlus sensor (Mode 1). (a) 2D FFT filtered image, (b) noise image, and (c) cross section of (a) for the tested piezoelectric MEMS sensor. (d) 2D FFT filtered image, (e) noise image, and (f) cross section of (d) for the qPlus sensor. The effective signal to noise ratios were determined as ≈ 2.6 for the MEMS sensor and ≈ 9.4 for the qPlus sensor. The imaging conditions (except of the oscillation amplitude) were identical for both sensors and can be found in the captions of Figure 5 and Figure S5. Amplitude of MEMS sensor ≈ 1.08 nm. Amplitude of qPlus sensor ≈ 50 pm.

For an objective comparison of the sensors, we determined their “effective signal to noise ratio” using a method illustrated in Ref.¹ Using a 2D FFT filter, the structural information of the images was separated from the image noise. This is exemplary shown for both sensors in Figure S6 (the corresponding raw images can be found in Figure 5(a) and Figure S5(a)). The 2D filtered and noise images as well as the corresponding scan lines for the MEMS sensor are shown in Figure S6(a), (b) and (c). The respective 2D filtered and noise images as well as the scanlines for the qPlus sensor are shown in Figure S6(d), (e) and (f). The effective signal-

to-noise ratio (SNR) was determined by dividing the standard deviation of the “signal” (i.e. a clean region without defects of the filtered image) by the standard deviation of the same region in the corresponding noise image. The determined effective SNRs for the STM images are ≈ 2.6 for the MEMS sensor and ≈ 9.4 for the qPlus sensor, respectively. Consequently, in case of STM topography images (FigureS6), the qPlus sensor up to date has a three to four times better signal to noise ratio compared to the MEMS sensor we tested.

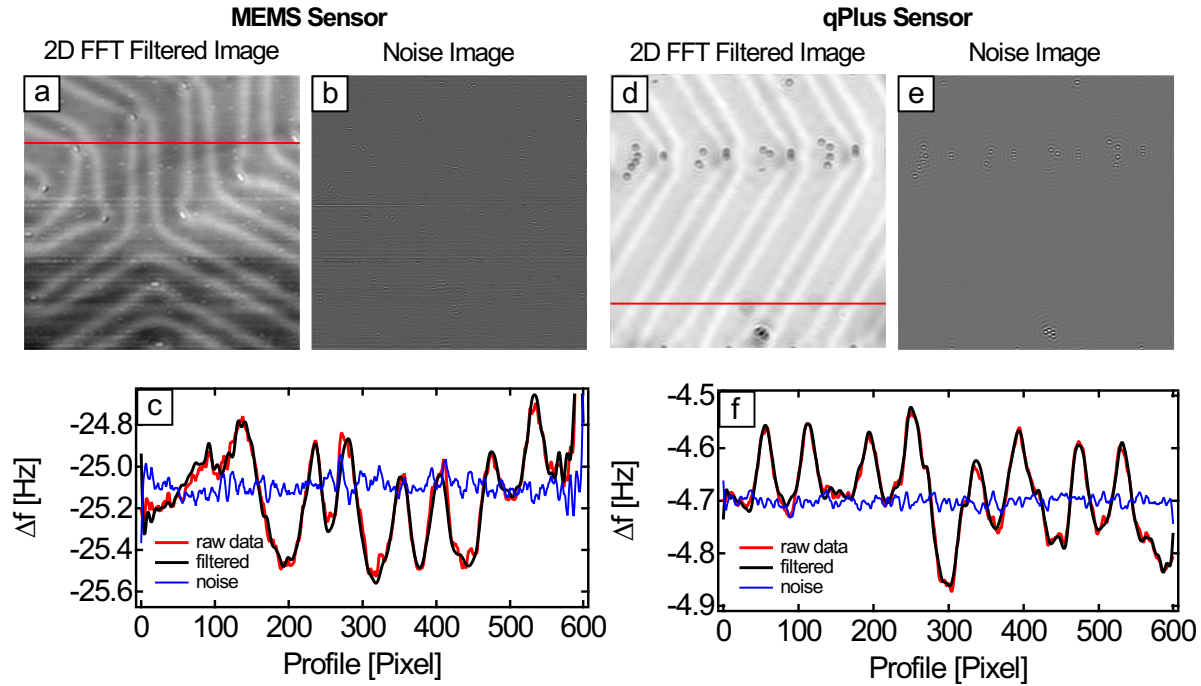


Figure S7: Effective SNR calculation from AFM frequency shift images. (a) 2D FFT filtered image, (b) noise image, and (c) cross section of (a) for the tested MEMS sensor. (d) 2D FFT filtered image, (e) noise image, and (f) cross section of (d) for the qPlus sensor. The effective signal to noise ratios were determined as ≈ 4.1 for the MEMS sensor and ≈ 5.8 for the qPlus sensor. The imaging conditions (except of the oscillation amplitude) were identical for both sensors and can be found in the captions of Figure 5 and FigureS5. Amplitude of MEMS sensor ≈ 1.08 nm. Amplitude of qPlus sensor ≈ 50 pm.

Figure S7 shows a similar comparison for the AFM frequency shift signals. In this case, the effective SNRs were ≈ 4.1 for the MEMS sensor and ≈ 5.8 for the qPlus sensor, respectively.

In TableS1 below we compare the effective SNRs for two different scanning speeds (see images in FigureS3(c),(h), FigureS4(c),(h), Figure 5(a),(b) and FigureS5(a),(b)). It can be seen that for low imaging speeds of 1.67 nm/s, the qPlus sensor has a 1.4 times better signal

to noise ratio in the AFM frequency shift compared to the MEMS sensor. However, for high imaging speeds of 25 nm/s, the MEMS sensor achieves a 1.3 times better signal to noise ratio in the AFM frequency shift compared to the qPlus sensor.

Table S1: Effective signal to noise ratios for the MEMS and qPlus sensors at different scanning speeds.

	STM Topography		AFM Frequency Shift	
	qPlus	MEMS	qPlus	MEMS
SNR at 1.67 nm/s (Figure 5, Figure S5)	9.4	2.6	5.8	4.1
SNR at 25 nm/s (Figure S3, Figure S4)	5.6	1.8	1.0	1.3

Note that all other images in this article as well as in the supplementary information are shown as unfiltered raw data. The 2D FFT filtering was only applied for determination of the noise in the images shown in Figure S6 and Figure S7.

References

- (1) Martin-Jimenez, D.; Ihle, A.; Ahles, S.; Wegner, H. A.; Schirmeisen, A.; Ebeling, D. Bond-level imaging of organic molecules using -controlled amplitude modulation atomic force microscopy. *Appl. Phys. Lett.* **2020**, *117*, 131601.